Proceedings of the ASME 2010 3rd Joint US-European Fluids Engineering Summer Meeting and 8th International Conference on Nanochannels, Microchannels, and Minichannels
FEDSM-ICNMM2010
August 1-5, 2010, Montreal, Canada

FEDSM-ICNMM2010-31271

EXPERIMENTAL AND CFD INVESTIGATIONS TO EVALUATE THE EFFECTS OF FLUID VISCOSITY AND PARTICLE SIZE ON EROSION DAMAGE IN OIL AND GAS PRODUCTION EQUPIMENT

Risa Okita
Risa-Okita@utulsa.edu

Yongli Zhang
Yongli-Zhang@utulsa.edu

Brenton S. McLaury
Brenton-McLaury@utulsa.edu

Siamack A. Shirazi*
Siamack-Shirazi@utulsa.edu

Edmund F. Rybicki*
Ed-Rybicki@utulsa.edu

Department of Mechanical Engineering, The University of Tulsa

ABSTRACT

Zhang et al (2006) utilized CFD to examine the validity of erosion models that have been implemented into CFD codes to predict solid particle erosion in air and water for Inconel 625. This work is an extension of Zhang's work and is presented as a step toward obtaining a better understanding of the effects of fluid viscosity and sand particle size on measured and calculated erosion rates. The erosion rates of Aluminum 6061-T6 were measured for direct impingement conditions of a submerged jet. Fluid viscosities of 1, 10, 25, and 50 cP and sand particle sizes of 20, 150, and 300 μm were tested. The average fluid speed of the jet was maintained at 10 m/s. Erosion data show that erosion rates for the 20 and 150 μm particles are reduced as the viscosity is increased, while surprisingly the erosion rates for the 300 μm particles do not seem to change much for the higher viscosities. For all viscosities considered, larger particles produced higher erosion rates, for the same mass of sand, than smaller particles. Concurrently, an erosion equation has been generated based on erosion testing of the same material in air. The new erosion model has been compared to available models and has been implemented into a commercially available CFD code to predict erosion rates for a variety of flow conditions, flow geometries, and particle sizes. Since particle speed and impact angle greatly influence erosion rates of the material, calculated particle speeds were compared with measurements. Comparisons reveal that, as the particles penetrate the near wall shear layer, particles in the higher viscosity liquids tend to slow down more rapidly than particles in the lower viscosity liquids. In addition, CFD predictions and particle speed measurements are used to explain why the erosion data for larger particles is less sensitive to the increased viscosities.

1. INTRODUCTION

Oil and gas, produced from reservoirs, usually contain impurities such as sand particles. The sand particles impinge the wall of flow lines and remove material from the pipe wall. The removal of material by solid particles is called erosion. The erosion damage caused by particles can be very dangerous since pipes and fittings can rupture suddenly without prior indication of failure. Failures caused by erosion also can result in expensive repairs and lost production time. In order to save money and increase safety, many industries are using erosion models to predict when the pipeline and fittings are susceptible to significant erosion damage.

In the literature, there are many equations developed to predict solid particle erosion [1-4]. The erosion equations normally depend on particle impact speed and angle, particle and material properties. However, in various flow situations fluid properties affect particle impact speed and angle. Therefore Computational Fluid Dynamics (CFD) is normally used to predict particle impact speed and angle so that this information can be used in erosion models to predict solid particle erosion [5-7]. Previously, Zhang et al. (2006) conducted a series of erosion measurements and calculations to show that erosion equations can be utilized in CFD software to predict erosion. They conducted a series of erosion tests in gas and developed a representative erosion equation. Next, the erosion equation was implemented into a commercially available CFD code and used to predict erosion for various gas and liquid cases. However, their study was

* ASME Fellow

limited to only one sand particle size and only erosion resulting from sand in either air or water was considered in direct impingement flow geometry [5, 6]. In order to extend the previous work and predict the amount of erosion resulting for various viscous liquids and particle sizes, several investigators have measured speeds of particles and carrier fluid, as well as erosion rates for the direct impingement flow geometry for a range of carrier fluid viscosities and sand particle sizes [8, 9].

The tasks and steps in the present work are shown in Figure 1. CFD based erosion calculations in this work includes the following steps and contributions: (1) Flow speed calculations and particle tracking are performed in the CFD program. Flow calculations provide flow information such as fluid speeds and pressure. Particle tracking calculations provide particle information, such as particle speeds and particle impact conditions. (2) Flow and particle speeds are validated by measuring the actual fluid and particle speeds in the direct impingement geometry for liquids with different viscosities utilizing Laser Doppler Velocimetry (LDV). (3) Erosion data were collected for 6061-T6 aluminum target material and various particle types in air for the same flow geometry. Erosion models were generated to represent these conditions. (4) Erosion data for the same aluminum material was collected for the same particle types and geometry in liquids with various viscosities. (5) Erosion rates in liquid are calculated in CFD applying the erosion models from Step (3). Once again at this stage, the CFD predicted erosion rates are validated by comparisons with actual erosion measurements from step (4).

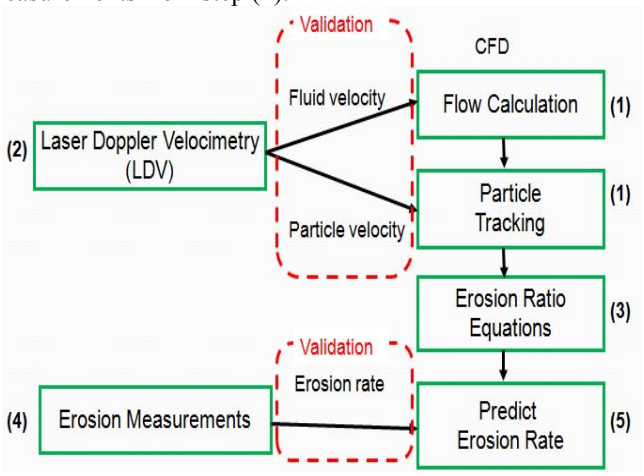

Figure 1: Flow Chart of Erosion Prediction Using CFD

2. EROSION RATIO EQUATIONS

Many investigators have studied erosion mechanisms and found that erosion is influenced by various factors such as particle size, particle impact speed, impact angle, target material properties such as density, hardness, and many other factors [10-14]. Erosion can be very complex, since erosion is influenced by so many factors. Meng and Ludema (1995) studied previous erosion models and equations in the literature and concluded that there is no universal model which works for all flow conditions or materials for practical uses [11]. Since there is no universal model which works for all materials or flow conditions, an erosion model must be developed for each material and condition separately.

Two erosion equations are used in this paper to predict the erosion ratio for aluminum 6061-T6. Equation (1) is called the E/CRC (Erosion/Corrosion Research Center) equation and originally presented by investigators of E/CRC for carbon steels (McLaury (1993) [2]) but is modified in this work. The equation calculates the erosion ratio based on particle impact angle and speed as well as material Brinell hardness. ER is the erosion ratio in kg of material loss per 1 kg of sand through put. F_s is a sharpness factor which ranges from 0.2 to 1 and depends on the shape of sand particles. C and n are the empirical constants. In literature, n is found to be between 2.0 to 2.9 [5, 6, 10, 12]. In this work 2.41 is used for n. BH is the Brinell hardness of the target material calculated based on Vicker's hardness of the material using Equation (3). V is the impact particle speed and f(θ) is the function of impact angle shown in Equation (2). This equation is a modified version of the one originally proposed by Oka et al. [3, 4].

$$ER\left(\frac{kg}{kg}\right) = F_s * C(BH)^{-0.59} * V^n * F(\theta) \quad (1)$$

$$F(\theta) = \frac{1}{f} * (\sin\theta)^{n_1} * (1 + Hv^{n_3}(1 - \sin\theta))^{n_2} \quad (2)$$

$$BH = \frac{(H_v + 0.1023)}{0.0108} \quad (3)$$

Equation (4) is the erosion model developed by Oka et al. in 2005 [3, 4]. K, k1, k2, k3 are the constants based on particle properties and hardness of target material. ρ is the density of the target material. V' and D' are reference values based on experiments (104 m/s and 326 μm respectively). F(θ) is the angle function and is shown in Equation (5). The difference between the forms of Equations (2) and (5) is that there is an additional constant, n_3, as an exponent to the Vicker's hardness in Equation (2).

$$ER\left(\frac{kg}{kg}\right) = K * (H_v)^{k1} * \left(\frac{V}{V'}\right)^{k2} * \left(\frac{D}{D'}\right)^{k3} * \rho * F(\theta) \quad (4)$$

$$F(\theta) = (sin\theta)^{n_1} * (1 + H_v(1 - sin\theta))^{n_2} \quad (5)$$

Values for the constants in each equation are shown in Table 1. E/CRC equation is defined for two types of sand with particle sizes of 150 and 300 μm. Oka developed the erosion equation based on air testing. The E/CRC equation is also developed based on direct impingement testing in air. The details of how the E/CRC equation was developed are shown in the next section. The erosion equation developed through gas testing is used to predict erosion for a liquid carrier fluid. Using the particle information such as particle speed and angle for each impingement from CFD, total erosion of the target material are calculated.

Table 1: Constants for Erosion Equations (Aluminum 6061)

Oka's Equation		Present Work (E/CRC)		
Variables	**Values**	**Variables**	**150 µm**	**300 µm**
Hv (Gpa)	1.12	**Hv (Gpa)**	1.12	1.12
k	65	**F_s**	0.5	1
k1	-0.12	**f**	5.27	2.19
k2	$2.3(Hv)^{0.038}$	**n1**	0.59	0.5
k3	0.19	**n2**	3.6	2.5
n1	$0.71(Hv)^{0.14}$	**n3**	2.5	0.5
n2	$2.4(Hv)^{-0.94}$	**C**	1.50E-07	3.28E-07

3. EXPERIMENTAL FACILITY AND CONDITIONS

3.1 Experimental Facility – Liquid Testing

An experimental facility was constructed to measure erosion for carrier fluids with different viscosities and different particle sizes. Figure 2 shows a schematic of the experimental facility. The viscous liquid is made in the reservoir tank prior to conducting the experiments by mixing CMC (Carboxymethyl Cellulose) and water. The density of the mixture was essentially the same as the density of water. The viscosities of the carrier fluid tested were 1, 10, 25, and 50 cP. The CMC-water mixture is known to be a non-Newtonian fluid; however, at the low viscosities of the current test conditions, the CMC-water mixture behaves as a Newtonian fluid. Sand particles are mixed with liquid in the reservoir tank. The ratio of sand particles and liquid are usually 0.1 % by volume. The slurry mixer is turned on while taking measurements in order to maintain the homogeneity of the mixture. The mixture of sand and liquid travels from the reservoir tank to the hydraulic pump and from the pump to the straight nozzle in the testing tank. The bypass valve is used to control the flow rate in the system during the measurements. Mixtures exit the nozzle and impinge the target wall and drain from the testing tank back to the reservoir tank. The mixture circulates in the system. The nozzle and target wall are completely submerged in the mixture. The nozzle diameter is 8 mm, and the distance from nozzle exit to the wall is 12.7 mm. The average fluid speed at the nozzle exit was kept at 10 m/s.

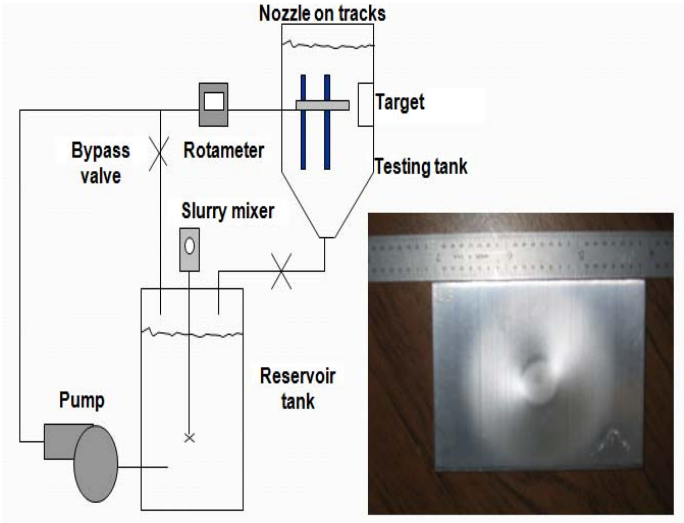

Figure 2: Schematic of the Experimental Facility

Flat surface coupons shown in Figure 2 are used to measure the erosion at the target wall. The weight of a coupon is measured before and after each test to determine the metal weight loss (kg). The weight loss of material is divided by mass flow rate of sand in the system, $\dot{M}_{sand}$ (kg/s) and testing time, t_{test} (s) to calculate the erosion mass ratio (kg/kg). The erosion mass ratio (kg/kg) is then divided by the density of the target wall to obtain erosion volume to mass ratio (m^3/kg). The calculation is shown in Equation (6)

$$ER_{vol}\left(\frac{m^3}{kg}\right) = \frac{W_{before} - W_{after}}{\dot{M}_{sand} * t_{test} * \rho} \quad (6)$$

The types of sand used for testing are silica flour, Oklahoma #1 sand and California 60 sand. The average particle sizes are 20, 150, and 300 µm, respectively. Microscopic pictures of these sand particles are shown in Figure 3. Silica flour and California 60 sand have sharper particles than the Oklahoma #1 sand.

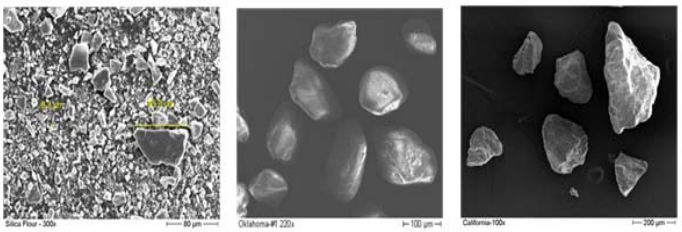

Figure 3: Microscopic Pictures of Abrasive Particles

3.2 Experimental Facility – Air Testing

The erosion model for aluminum 6061-T6 is developed based on direct impingement test results in air. Air is used as the carrier fluid to generate erosion equations since in such low viscosity fluids, the particle speed and direction do not

change much as particles approach the target wall; therefore, it is easy to control particle impact speed and angle. Figure 4 is a schematic of the direct impingement testing in air. A compressor provides the air flow in the nozzle. The flow rate of the gas was controlled by the valve positioned upstream of the flow meter. Sand is injected from the sand feeder. The pressure drop at the nozzle creates suction in the feeding tube and draws the sand particles in the nozzle. The mixture of the sand and air flow out of the nozzle, and particles impinge the target material.

In air, it is common that there is a relative slip velocity between a particle and the gas. So, the particles leaving the nozzle are traveling at a lower speed than the gas at this location. The particle speeds, V_p, of 150 and 300 µm particles are measured by LDV and the gas speeds were measured by a Pitot tube. The Pitot tube was installed at the center of the nozzle approximately 3 mm downstream of the nozzle exit. The measured gas speed at this location by the Pitot tube was divided by 1.2 (assuming fully developed turbulent pipe profile) to obtain an approximate average gas speed across the nozzle exit. The gas speed was measured before sand was injected in the system and the measured gas speeds are not influenced by the sand particles. It should be noted that Pitot tube is only used as a reference for calibration and the gas velocities that are measured by the Pitot tube may not accurately represent the average gas speed at the nozzle exit and they are not used in any calculations. The graph of the particle vs. gas speed is shown in Figure 4. As shown in the graph, the particle speed is directly proportional to the fluid speed. A linear equation was used to extrapolate between data points. The data show that there is more slip between the fluid and the particles for the 300 µm particles than for the 150 µm particles. The linear equations in Figure 4 were used to determine the gas speeds necessary to produce the desired particle speeds during the erosion measurements. It should be noted that, for these larger particles entrained in a gas, only axial velocities at the nozzle exit were measured. For larger particles flowing in a gas, CFD results as well as observed erosion patterns on the specimens indicate that the momentum of the particles near the target wall are not affected by the gas speed.

After the particle speeds were measured, the erosion measurements were conducted for aluminum 6061-T6 in air. From the LDV measurements, particle speeds of 13, 24, and 42 m/s were chosen as particle speed conditions. At each speed, measurements were taken for impact angles of 90, 60, 30, and 15 degrees. At each particle speed and angle, the measurements were taken at least 3 times with 300 grams of sand each time. Erosion ratios (kg/kg) are calculated by mass loss of a target coupon (kg) divided by the total mass of sand throughput (kg). Particle sizes of 150 and 300 µm are used as abrasive sands for these measurements.

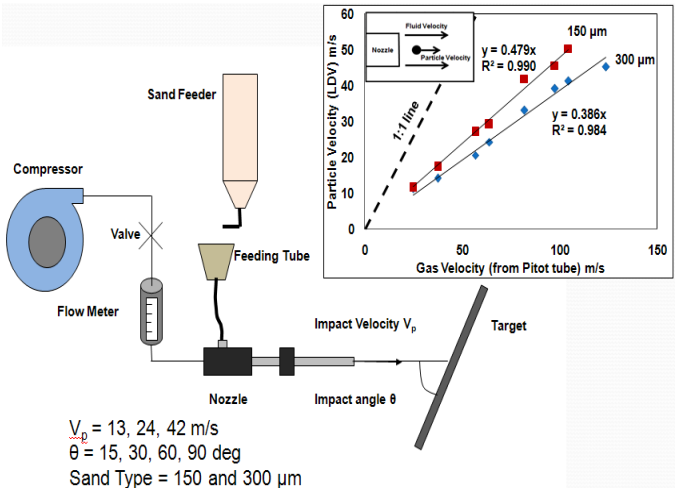

Figure 4: Schematic of Erosion Measurements in Air

3.3 LDV Measurement Conditions

Particle axial and radial speeds and liquid axial and radial speeds were measured utilizing LDV by Miska [8]. Aluminum particles with the average sizes of 3, 120 and 550 µm were used as seeding particles. 3 µm particles were assumed to travel with liquid with no slip. 120 and 550 µm particles were used to measure the speeds of small and big particles. Figure 5 shows the measurement locations between the nozzle exit and the target wall. The measurements were performed for r = 0 to r = 12 mm and z = 1 to z = 12.3 mm. The particle speeds could not be measured near or on the target surface (z = 12.7 mm) since the measuring section of LDV (control volume created by laser beams intersections) is 0.2 mm wide and any location within 0.2 mm of the wall, the wall would interfere with the measurement.

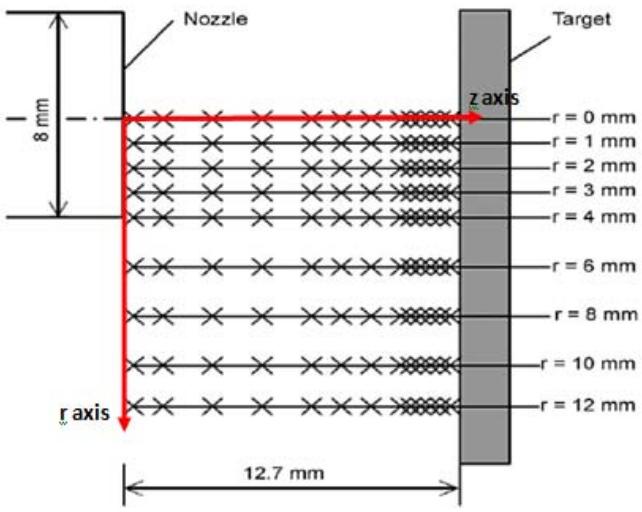

Figure 5: LDV Measurement Location Map

Measurements were collected for 5 different viscosities of 1, 10, 25, 50, and 100 cP. Since the CMC-water mixture is turbid and does not allow laser beams to pass through the measurement section, glycerin was mixed with water to attain the desired viscosities of the carrier fluids for these experiments.

4. CFD APPROACH AND DESIGN INPUT

Computational Fluid Dynamics (CFD) was utilized to predict fluid and particle speeds and erosion ratio of aluminum 6061-T6 for various viscous liquids to evaluate the accuracy of the erosion models generated from air testing. Fluent 6.3 was used for flow simulations and particle tracking. Erosion ratios are calculated by User Defined Functions (UDF) created by Zhang et al. (2006) [5].

The computational mesh of the direct impingement case is shown in Figure 6. This geometry is modeled as two-dimensional axi-symmetric. The diameter of the entire flow region is 38.1 mm and its length is 25.4 mm. The nozzle diameter is 8 mm, and the distance to the wall is 12.7 mm which is the same as the experimental apparatus. In the flow region, the grid gets finer near the target wall. The total number of cells used for this geometry is 4600. For the nozzle exit plane speed, actual LDV data are used for the inlet speed condition. The Reynolds Stress Model (RSM) is used to calculate the flow field, and the standard wall function is used to simulate the flow near the target wall.

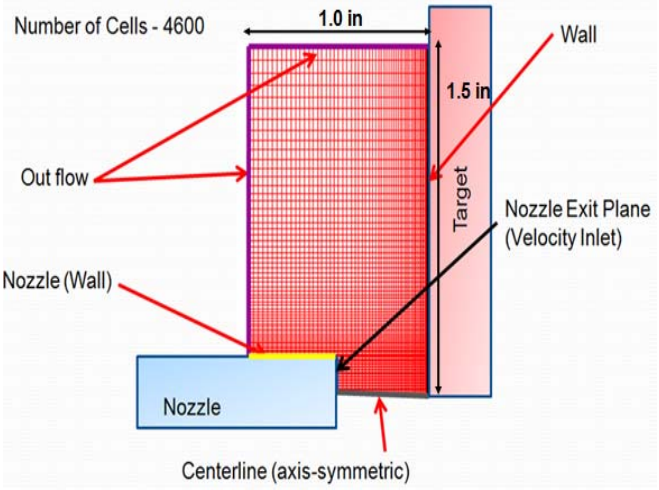

Figure 6: CFD Mesh of the Flow Region and Boundary Conditions.

5. CFD AND EXPERIMENTAL RESULTS

5.1 Measured Erosion Results in Viscous Liquids

Figure 7 presents the measured erosion volume to mass ratio with change in viscosity of carrier fluid for aluminum 6061-T6. Table 2 summarizes the erosion results for the coupon tests. More than two measurements were taken for each condition for 150 and 300 µm particles and results were averaged. One measurement was taken for 20 µm particles. The standard deviation for each test condition in Table 2 shows the range of the measurements and indicate repeatability. Figure 7 shows erosion ratio is reduced as the viscosity increases for 20 and 150 µm particles. However, for 300 micron particles, the erosion ratio does not change as significantly as the viscosity is increased. The erosion ratio of 20 micron sand declines more significantly than that of 150 micron sand. From Table 2, it should be noted that the larger particles tend to have larger erosion ratios than smaller particles at any viscosity.

Table 2: Erosion Results for Al6061 (Coupon Tests)

Erosion Ratio (m^3/kg)					
Viscosity (cP)	Aluminum 6061				
	300 µm		150 µm		20 µm
	Value	STDV	Value	STDV	Value
1	1.19E-09	1.62E-10	5.43E-10	8.07E-11	3.62E-11
10	9.49E-10	3.01E-11	3.96E-10	3.41E-11	1.42E-11
25	9.95E-10	6.71E-11	2.63E-10	2.54E-11	8.50E-12
50	1.05E-09	1.50E-10	1.59E-10	8.84E-11	4.72E-12

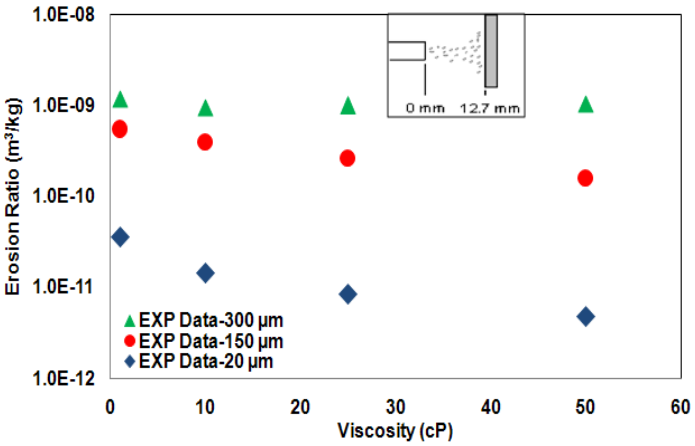

Figure 7: Erosion Ratio vs. Viscosity for Aluminum 6061 with Different Particle Size

5.2 Measured Erosion Results in Air

To develop the coefficients that are needed in the erosion equation (Eq. (1)), erosion ratios (kg/kg) are measured for aluminum 6061 T6 in air. This material is also used in erosion tests involving liquids. Oklahoma #1 (150 µm average size) sand and California 60 (300 µm average size) sand are used as abrasive particles. A total of 900 grams of sand was injected for the erosion tests that are presented in this section. After injecting each 300 g of sand, the weight of the coupon was measured and recorded.

Figure 8 and Figure 9 are the graphs of erosion ratio for aluminum 6061 in kg/kg vs. impact angle for three different impact speeds. For both particle sizes, higher particle impact speeds yield higher erosion ratios for all of the impact angles. From the figures, it is also found that erosion ratios are higher for lower impact angles for all the particle speeds. 300 µm particles give higher erosion ratios than 150 µm due to their size and shape. The microscopic pictures of these particles are shown in Figure 3. Note that the 300 µm particles erosion ratios have a trend that is slightly different from that of the 150 µm particles. Erosion ratios for the 150 µm particles increase more significantly as the impact angle decreases, while the erosion ratios for the 300 µm sand particles do not increase as significantly as for the 150 µm sand particles. The differences in the two types of sand can result in not only a difference in magnitude but also in trend of erosion ratio with impact angle (angle function).

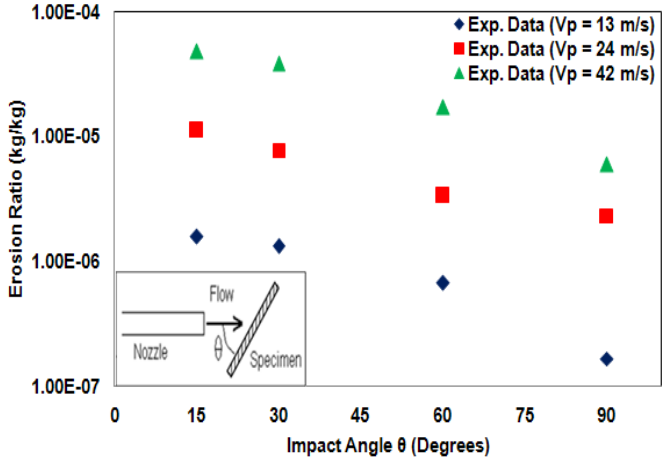

Figure 8: Erosion Ratio vs. Impact Angle for Al 6061 in Air (150 µm)

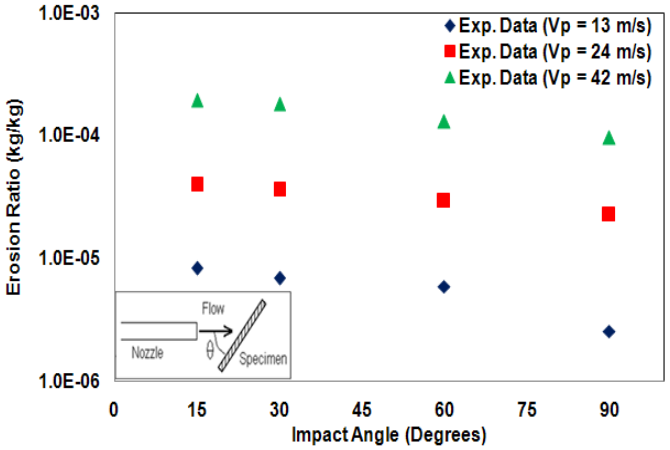

Figure 9: Erosion Ratio vs. Impact Angle for Al 6061 in Air (300 µm)

Utilizing the information gained through erosion measurements in air, the erosion model for aluminum was generated. At first, all the experimental results from Figures 8 and 9 are normalized and plotted together in Figure 10. The erosion ratio for each test condition is normalized by dividing it by the value of erosion ratio at θ = 15 degrees for each velocity (Eq. (7)). Since the results are normalized, the results for different particle speeds are close in value to each other which indicate that particle speed only affects the erosion equations in magnitude but not the shape of the erosion versus impact angle profile. The angle function shown in Equation (2) is defined by finding n1, n2, and n3 which fit the experimental data. Since the experimental data are normalized, the angle function must be normalized as well by dividing the function by f, which is the maximum value of the function.

$$ER_{normalized}(-) = ER\left(\frac{kg}{kg}\right) / ER_{\theta=15}\left(\frac{kg}{kg}\right) \quad (7)$$

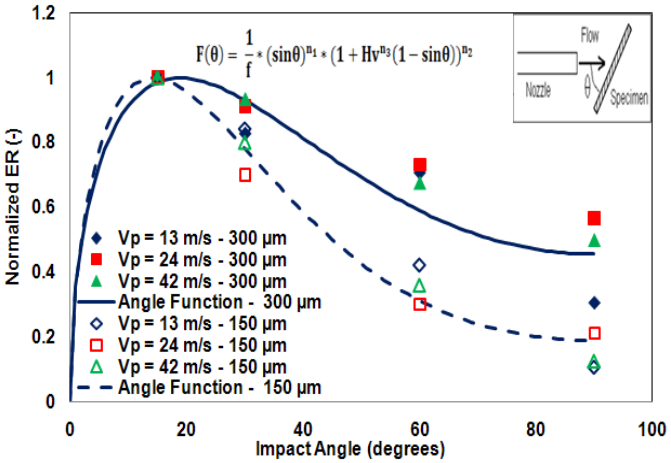

Figure 10: Normalized Erosion Ratio vs. Impact Angle in Air – 150 and 300 µm

After the angle functions are defined, the erosion equations are defined by finding an empirical constant C for each sand type. These constants are listed in Table 1. Figures 11 and 12 are the measured erosion ratio vs. impact angle for 13 m/s plotted with the newly defined E/CRC equation and Oka's equation. For 150 µm particles, the new E/CRC equation tends to give higher erosion ratios at lower angles than Oka's equation. However, at higher angles, from 50 to 90 degrees, erosion ratios given by Oka's equation are higher than the E/CRC equation (Figure 11). For 300 µm particles, Oka's model gives much lower erosion ratios than the new E/CRC equation (Figure 12). This is because there is no parameter that accounts for sharpness in Oka's equation. There is a factor, k3, which accounts for the size of particle, but it is very small, therefore, there is not much difference in the erosion ratios predicted by Oka's model for the 150 and 300 µm particles in this equation. On the other hand, the new equation is generated based on erosion testing in air for 300 µm sand; therefore, it is more accurate than Oka's equation. The erosion equations for 150 and 300 µm particles defined here are used in the CFD code to predict erosion ratios for the liquid testing.

Since there is no erosion data for 20 µm particles, the erosion equation for 150 µm particles is used to predict erosion ratios for this sand. Sand sharpness factor of 1 is used instead of 0.5 since 20 µm sand has much sharper edges than the 150 µm sand (Figure 3).

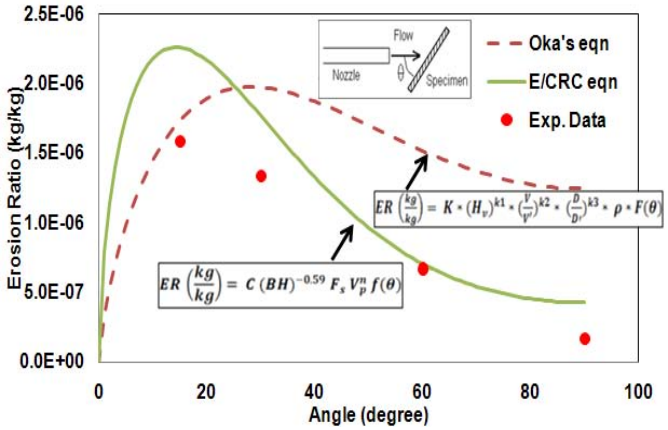

Figure 11: Erosion Ratio vs. Impact Angle at V = 13 m/s (150 µm, Aluminum)

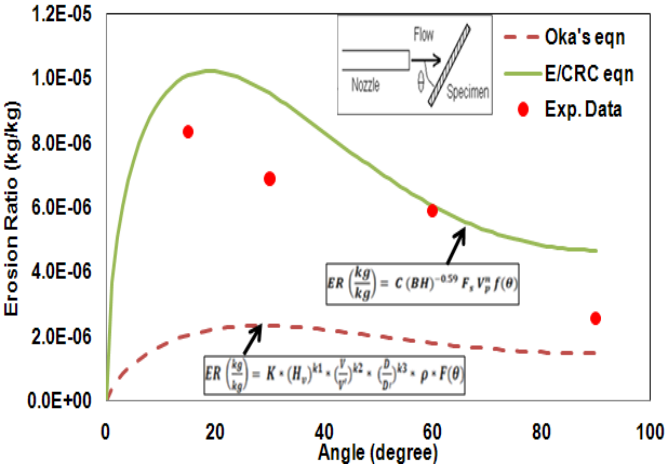

Figure 12: Erosion Ratio vs. Impact Angle at V = 13 m/s (300 µm, Aluminum)

5.3 Comparison of Predicted and Measured Particle Speeds

Although erosion is influenced by many factors, particle impact speed is the biggest factor that affects erosion. In order to study the effect of viscosity and particle size on particle speed, which affects erosion ratio, axial and radial particle speeds of 3, 120 and 550 µm diameter particles were measured in 1, 50 and 100 cP fluid viscosities and compared to the CFD predicted speeds. Note that the results shown in this paper are speeds that are magnitudes of the velocity vectors calculated from axial and radial velocity components. The predicted particle impact speed and angle are used in CFD to calculate erosion ratios. Therefore it is important to compare calculated particle speeds with experimental data to make sure that calculated particle speeds match the data.

Figure 13 shows the contour plots of 120 µm particle speeds for 1 and 100 cP. The contours show a high speed near the nozzle exit along the horizontal axis (centerline). The speeds in this region (marked by the red oval) are mostly in the axial direction (small radial speed) which travel from

nozzle exit toward the target metal. The speeds near the centerline for the 100 cP fluid are higher than the speeds in the same region for the 1 cP fluid. For the same flow rate, the 100 cP fluids have a laminar profile at the nozzle exit while the 1 cP fluid has a turbulent profile; thus the maximum speed in this region tends to be higher for higher viscosity liquids. However, the particles slow down as they approach the wall due to the reduction in fluid speed at the stagnation point. As particles move radially away from the centerline along the target wall, there is another location with high particle speed (shown by the black oval). The speed of particles in this region is high and is mostly from the radial component of speed which travels outward from the centerline. These high speeds are responsible for erosion that occurs in this region.

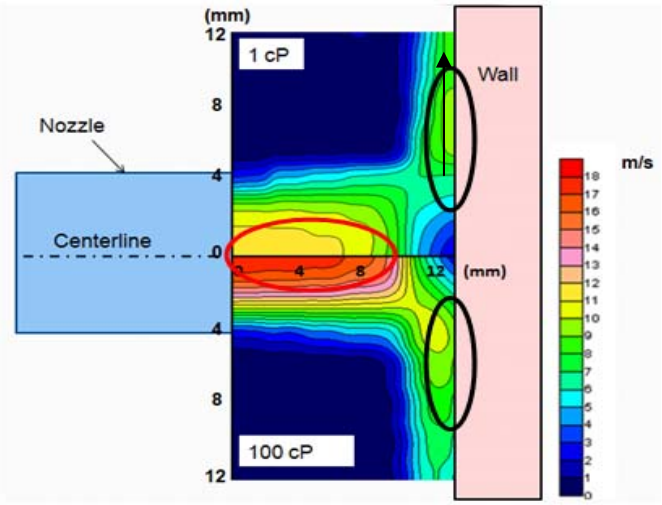

Figure 13: Contour plots of particle speed for 120 µm (1 and 100cP)

Figure 14 presents the measured particle axial speeds of 120 and 550 µm particles at z = 1 mm. This location is the first location measureable by LDV outside the nozzle. The particle axial speeds measured at this location are used as speed inlet conditions for CFD particle tracking simulations. The radial particle speed at this location is very small. From Figure 14, it is observed that particle speeds in the higher viscosity liquids have higher speeds near the centerline. This is due to the reduction in Reynolds number due to the increased viscosity. 550 µm particles tend to travel with slightly lower speeds than 120 µm particles due to slip.

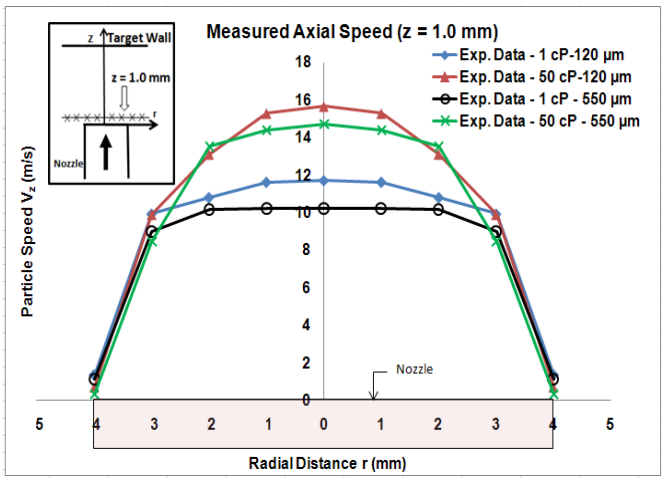

Figure 14: Measured Particle Speed V_z at z = 1 mm

Detailed comparisons of measured and predicted speeds for 120 µm particles along r = 0 and 8 mm are shown in Figures 15 to 17. Results for 550 µm and the other radial locations are omitted here since the comparison of 120 and 550 µm particle speeds will be shown in the following section.

As shown in Figure 15, particle speeds at the centerline (r = 0 mm) are higher for higher viscosity fluids than that of lower viscosity fluids at the nozzle exit (z = 0 mm). However, as particles approach the wall, speeds decrease and become negligible at the wall. The particle speeds along the centerline are axially dominant which means most of the particles are traveling in the horizontal direction towards the wall. For r = 0 mm, CFD predictions match the measured speeds.

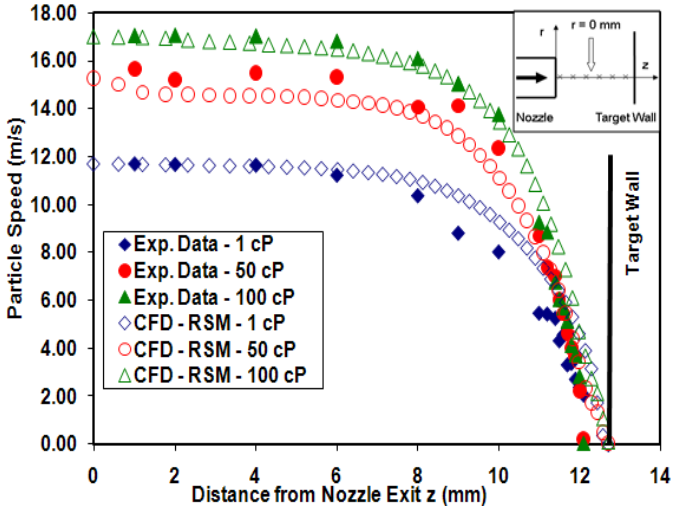

Figure 15: Measured and Predicted Particle Speeds vs. Axial Distance at r = 0 mm – 120 µm

For r = 8 mm, the particle speeds are low at the nozzle exit (z = 0 mm); however, they increase near the wall and reach a maximum speed, then decrease again very close to the wall (Figure 16). Although the particle speeds become

smaller as they approach the wall, they never become zero. The erosion is caused by this non-zero particle speed at the target wall. The particle speeds in this region are mostly radial and the axial velocity components are small, and particles move nearly parallel to the target wall. CFD predictions agree with the measurements for a location away from the wall, but CFD under- predicts speeds near the wall.

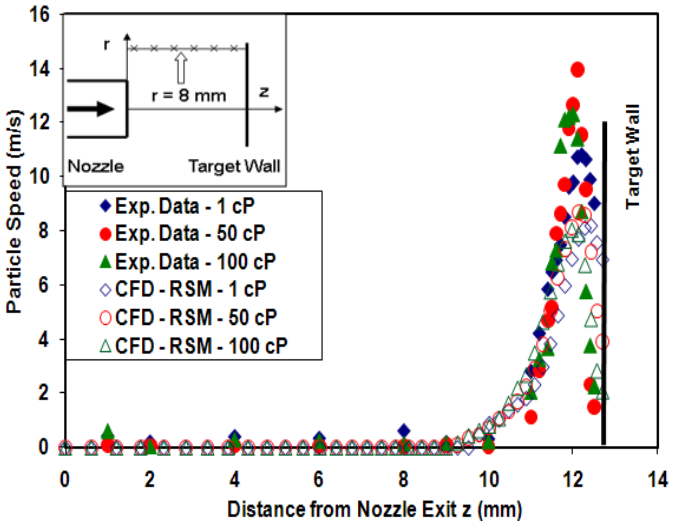

Figure 16: Measured and Predicted Particle Speeds vs. Axial Distance at r = 8 mm – 120 µm

In order to examine near wall particle behavior, Figure 16 is expanded from z = 10 to 12.7 mm (Figure 17). Figure 17 shows that both measured and predicted particle speeds reach their maximum values near the wall, and then particles slow down as they approach the wall. The location of maximum particle speed occurs farther away from the wall for higher viscosity liquids than for lower viscosity liquids. This can be explained by the fluid shear layer formed near the wall. The layer tends to be thicker for higher viscosity fluids than lower viscosity fluids. Particle speeds are influenced by these shear layers near the wall, and they slow down quickly as they enter these shear layers. Therefore, particles in higher viscosity liquids tend to slow down starting at a distance farther away from the wall than particles in lower viscosity liquids. Another thing to note here is that away from the wall, particle speeds in high viscosity fluids are higher than low viscosity fluids. However very near the wall, particle speeds in lower viscosity fluids are higher than speeds of higher viscosity fluids. As particles enter the shear layer near the wall, the higher viscosity liquids exert more drag on particles than lower viscosity fluids; as a result, particles in higher viscosity liquids slow down more significantly than particles in lower viscosity fluids. Also, since the shear layer as well as the distance between the maximum fluid speed and the wall are thicker for higher viscosity liquids, it provides a larger distance for the particles to slow down before they reach the wall. This explains why erosion ratios reduce as liquid viscosity is increased for small particles. CFD predicted speeds for each viscosity show the exact same trend.

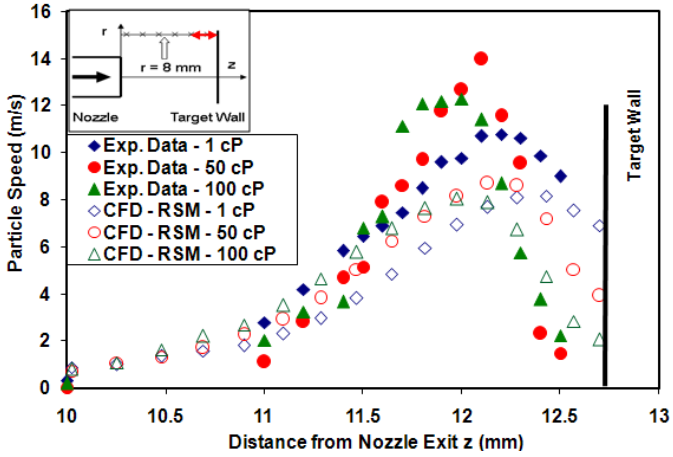

Figure 17: Measured and Predicted Particle Speeds vs. Axial Distance at r = 8 mm – 120 µm (Near Wall)

Figure 18 presents the comparison of the measured speeds of 120 and 550 µm particles in 1 and 50 cP fluids. 100 cP results are omitted here since they have similar profiles as 50 cP results. Figure 19 is the comparison of the predicted speeds of the same sizes of particles. Figure 18 shows that both 120 and 550 µm particles in 50 cP fluids reach maximum speed at locations further away from the wall than the particles in 1 cP. However, the difference of locations of maximum speed for 1 and 50 cP (distance between the two dash lines) is more obvious for 120 µm particles than for 550 µm particles. Also, near the wall, the differences of particle speeds in 1 and 50 cP (shown by arrows) are more significant for 120 µm particles than that of 550 µm particles. Predicted particle speeds in Figure 19 show the exact same trend.

The comparison of the length of the arrows (which represents the differences between the particle speeds) for the 550 and 120 µm particles graphs indicates that the particle speed does not change as much for 550 micron particles as for 120 micron particles when the viscosity of liquid changes from 1 to 50 cP. This is an indication that the speeds of larger particles are not affected by the fluid viscosity as much as those of smaller particles. The bigger particles have larger inertia than smaller particles, and they penetrate through the shear layer near the wall and do not slow down as much as smaller particles do. This is one of the reasons that erosion ratio does not change much with increase in viscosity for 300 µm sand.

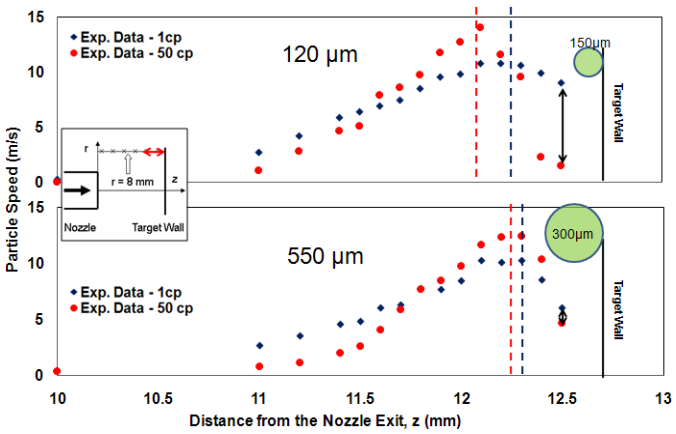

Figure 18: Measured Particle Speeds vs. Axial Distance at r = 8 mm – 120 and 550 µm (Near Wall)

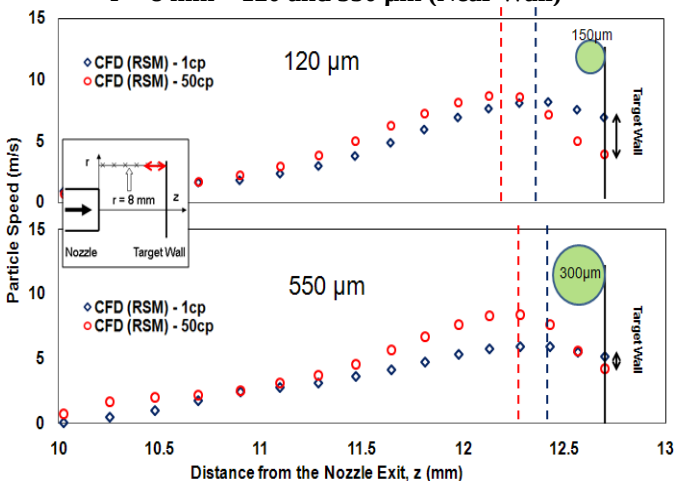

Figure 19: Predicted Particle Speeds vs. Axial Distance at r = 8 mm – 120 and 550 µm (Near Wall)

In order to examine how much particles are slowing down as they approach the wall, the particle acceleration with respect to axial distance, d(speed)/dz is calculated for each test condition. Figures 20 and 21 are the measured and predicted particle acceleration with respect to z vs. axial distance z along r = 8 mm near the wall. From both figures, it can be seen that both sizes of particles slow down significantly near the wall (negative values). Comparison of 1 cP and 50 cP profiles reveals that particles in 50 cP are slowing down more rapidly than particles in 1 cP. Comparison of two particle sizes show that 550 µm particles have lower deceleration than 120 µm particles near the wall.

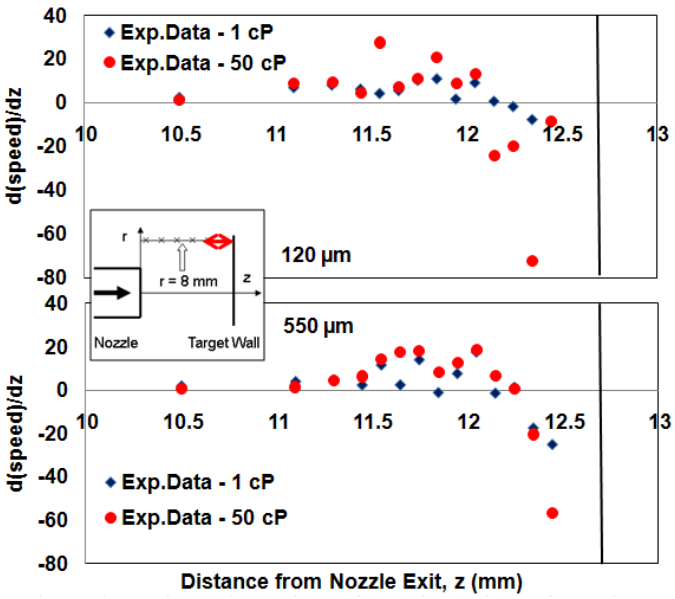

Figure 20: Measured d(speed)/dz vs. z Distance at r = 8 mm – 120 and 550 µm (Near Wall)

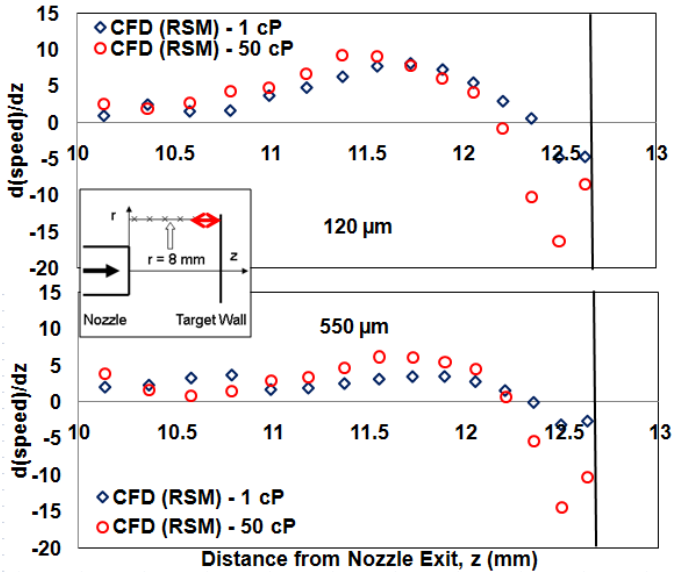

Figure 21: Predicted d(speed)/dz vs. z Distance at r = 8 mm – 120 and 550 µm (Near Wall)

In order to determine the dependency of results on the size of grid, a grid size analysis was performed. After the flow calculation was performed for the original mesh, the grid was made finer by breaking each cell into two cells in the z direction. A diagram of how the original grid is adapted to a finer grid is shown in Figure 22. The last layer of cells adjacent to the wall was kept the same so that it still fulfills the standard wall function criteria. The flow calculation was redone using the finer grid. Figure 23 is for particle speeds of 1 and 50 cP at r = 8 mm for the original and finer grids. To focus on the near wall speed, the horizontal axis of the plots is set from 6 to 12.7 mm in these figures. From Figure

23, it is observed that the particle speeds are independent of grid size for both 1 and 50 cP. Therefore, for this case, the results are not influenced by the size of mesh. The original mesh was used for all the predictions in this paper.

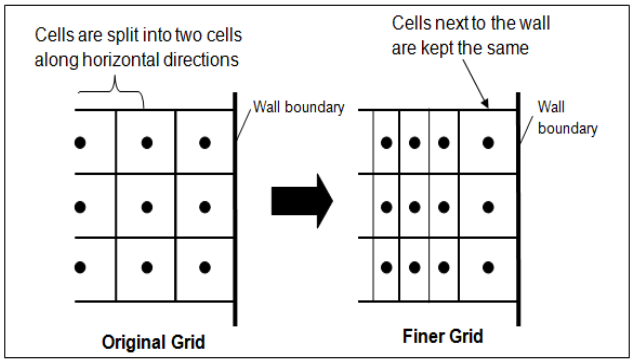

Figure 22: Diagram of Grid Adaptation

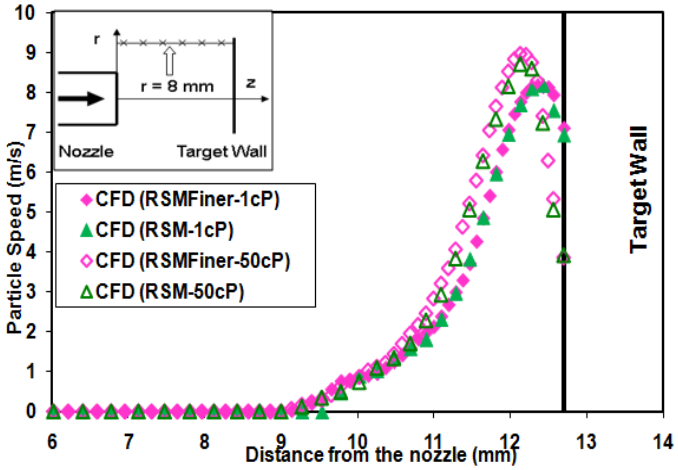

Figure 23: Comparison of Predicted Particle (120 µm) Speeds for Finer and Original Grid (1 and 50 cP)

5.4 Predicted Erosion Results in Liquid

After measuring the erosion ratio, erosion equations were utilized to predict erosion ratio for aluminum. Table 3 and Figures 24, 25 and 26 are the measured and predicted erosion volume to mass ratio of aluminum vs. viscosity for three particle sizes in units of m^3/kg. From Figure 24, CFD predicts that the erosion ratio decreases with increase in viscosity for 300 µm particles, while measurements show the erosion ratio stays constant across the viscosity change. The erosion ratio is also underpredicted by one order of magnitude by CFD for all the viscosities. The E/CRC model predicts better than Oka's model. Erosion ratio for 150 µm particles agree better with CFD predictions (Figure 25). Both predictions and measurements have declining profiles and the magnitude of erosion ratio is under-predicted only by a factor of 3 or 4. For this particle size, E/CRC and Oka's equations give similar values. For the smallest particles (20 µm), the predictions do not agree with the trend of measurements (Figure 26). Both equations predict that erosion ratio decreases from 1 to 10 cP, however, increases from 10 cP to 50 cP, while measurements show the erosion ratio is lower for higher viscosities. Also, for 20 µm particles, predictions are higher than measured values.

Table 3: Predicted Erosion Ratio for Aluminum 6061

Predicted Erosion Ratio (m^3/kg)						
Viscosity (cP)	Aluminum					
	300 µm		150 µm		20 µm	
	E/CRC	Oka	E/CRC	Oka	E/CRC	Oka
1	5.25E-10	1.26E-10	1.38E-10	1.14E-10	5.52E-10	1.14E-10
10	1.69E-10	4.15E-11	4.31E-11	3.39E-11	3.20E-10	7.94E-11
25	1.54E-10	3.70E-11	2.59E-11	2.11E-11	3.47E-10	9.56E-11
50	1.15E-10	2.77E-11	1.28E-11	1.14E-11	4.33E-10	1.28E-10

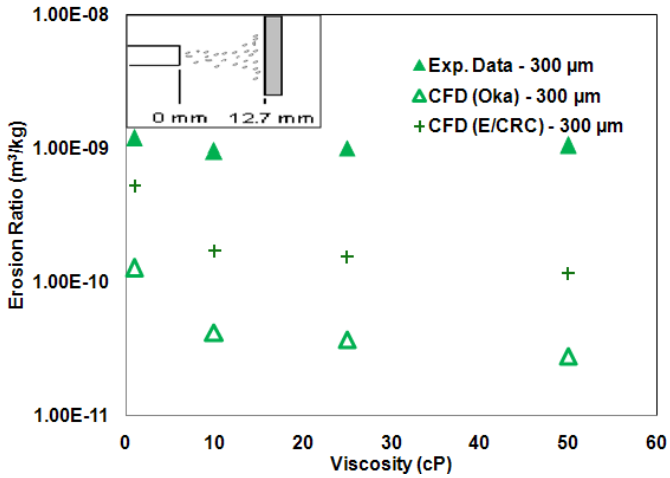

Figure 24: Predicted Erosion Ratio and Experimental Data for Aluminum (300 µm)

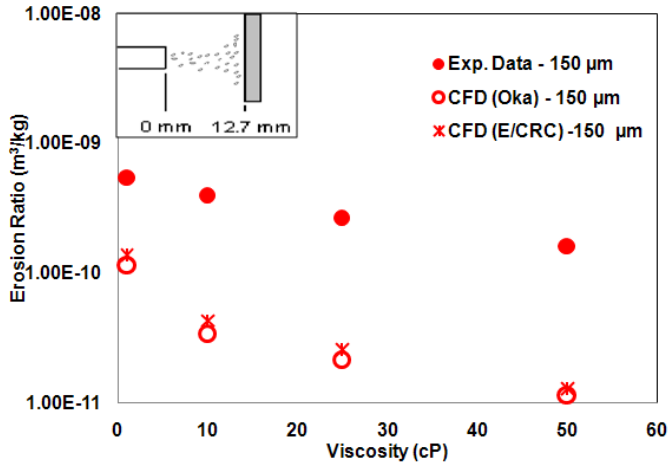

Figure 25: Predicted Erosion Ratio and Experimental Data for Aluminum (150 µm)

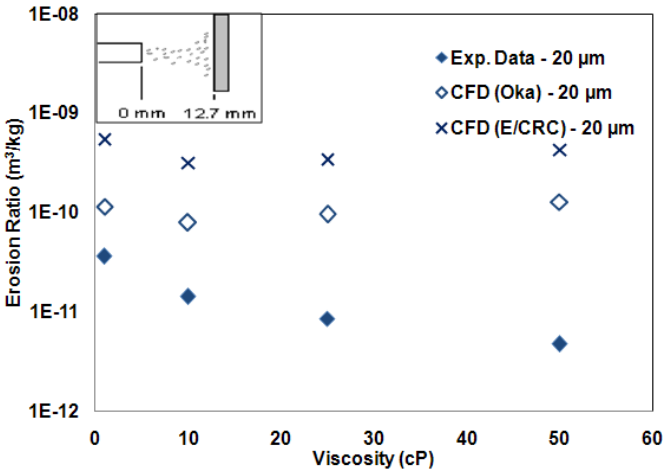

Figure 26: Predicted Erosion Ratio and Experimental Data for Aluminum (20 µm)

5.5 Number of Impacting Particles Analysis (CFD)

Besides particle speed, the number of impacting particles is another important factor that influences erosion ratio. As viscosity changes, the number of particles hitting the wall also changes. In CFD, 10,000 particles are released at the nozzle exit for each case, and the number of particles hitting the wall boundary was recorded using the UDF. The results are shown in Figure 27. Figure 27 shows the number of particles impacting vs. the number of impacts per particle for different particle sizes and different viscosities. Number of impacts (horizontal axis) is how many times each particle hits the wall. Number of particles impacting (vertical axis) is how many particles are hitting at each number of impacts. Some particles only hit the wall once or several times and move away from the shear layer near the wall (low number of impacts) while some particles keep hitting the wall over and over again and are stuck in the shear layer near the wall (high number of impacts). Figure 27 shows that 20 µm particles tend to have much higher number of impacts than 300 and 150 µm particles. For all particle sizes, a greater number of particles are hitting more frequently for higher viscosity liquids (50 cP) than in lower viscosity liquids (1 cP).

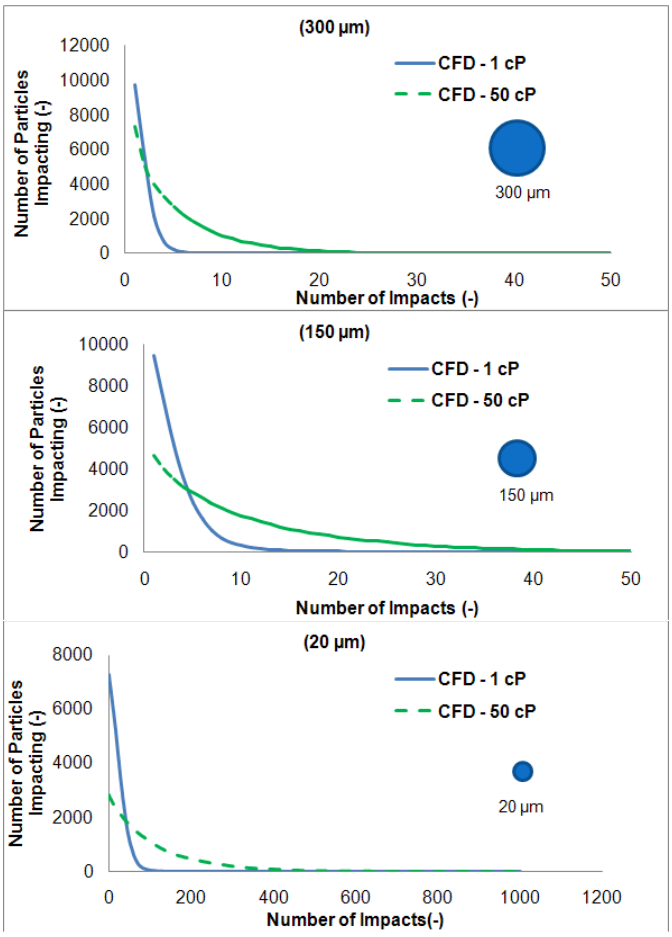

Figure 27: Number of Particle Impacting vs. Impact Number for 20, 150, and 300 µm

The number of impacts for 20 µm particles is very high as compared to other particles. To demonstrate that the number of particles impacting is the source of the difference between the CFD predictions and measurements, the erosion ratio for aluminum was recalculated for 20 µm particles using only the first impact and discarding the rest of the impacts for an individual particle. The results are shown in Figure 28. The graph shows the new CFD predictions using the first impact along with experimental data. The predictions using only the first impact agree with the experimental data much better than the original predictions using all of the impacts (Figure 26).

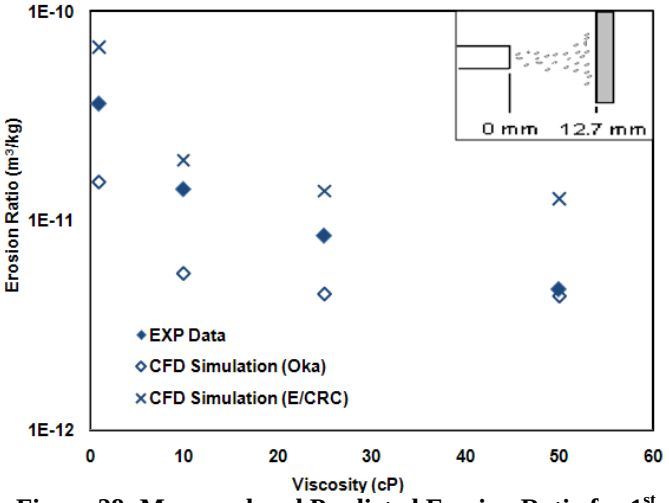

Figure 28: Measured and Predicted Erosion Ratio for 1st Impacts (20 µm, Al6061)

6. SUMMARY AND DISCUSSIONS

Erosion ratio for aluminum 6061-T6 occurring from 20, 150, and 300 µm particles with carrier liquids of 1, 10, 25, and 50 cP were measured. It was found that the erosion ratio decreases as viscosity increases for 20 and 150 µm sand while 300 µm sand showed no significant change in erosion ratio with change in viscosity.

Erosion models were developed based on air testing for the same aluminum. For aluminum, erosion models were generated for two types of sand: Oklahoma #1 and California 60. Each equation is unique with different empirical constants and angle functions. These newly developed equations were used to predict erosion ratio using CFD.

Erosion ratios in air and liquid were plotted against particle Reynolds number in Figure 29. Particle Reynolds number is a dimensionless number calculated using Equation (8). D_p is the diameter of particle, V_p is the particle velocity and ν is the kinematic viscosity of fluid. For liquid testing, each particle has different impact velocity and angle, therefore, average fluid nozzle exit velocity (10 m/s) is used for V_p for all the cases. For air testing, viscosity of room temperature air is used for all the test conditions.

$$Re_p = \frac{D_p V_p}{\nu} \quad (8)$$

From Figure 29, it should be noted that in both air and liquid, higher particle Reynolds numbers give higher erosion ratio which is intuitive. However closer examination reveals that air results have a steeper profile than liquid results. Also, for liquid testing, larger particles are not influenced by particle Reynolds number as much as smaller particles while in air, there is no significant difference in profile for 150 and 300 µm particles. Figure 29 also indicates that the particle Reynolds number is not the only parameter that influences erosion and other parameters such as local particle and fluid response times (perhaps local Stokes numbers) may affect erosion rates. This also may indicate that the erosion mechanism in liquid may be different from the one in air.

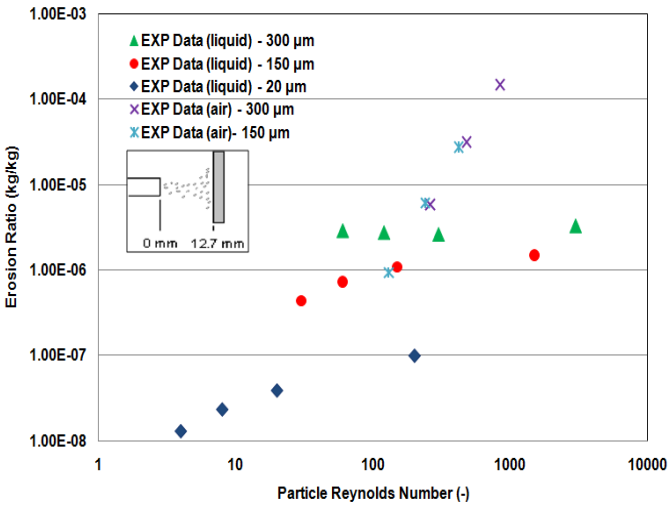

Figure 29: Erosion Ratio vs. Particle Reynolds Number

LDV measurements were examined in order to study how particles behave near the wall or target material. Fluid and particle speeds for 120 and 550 µm particles in 1, 50, and 100 cP fluids were measured. The comparison of predicted and measured particle speeds of small and large particles showed that CFD is able to predict speeds comparable to the measurements. Near the wall, however, it was found that the speeds of large particles are not affected by viscosity as much as that of small particles. Due to larger inertia, large particles penetrate through the shear layer near the wall and slow down but not as much as the small particles which slow down significantly as they enter the shear layer. As a result, erosion ratios with large particles do not change as much as small particles as viscosity changes. It was also found that higher viscosity liquids form thicker shear layers near the wall than lower viscosity liquids. Therefore, if particle sizes are the same, particles in higher viscosity fluids reach a maximum speed farther away from the wall and slow down more rapidly than particles in lower viscosity fluids near the wall. Since higher viscosity liquids have a thicker shear layer and exert higher drag on particles, particles impacting the wall have lower speeds in higher viscosity fluids than lower viscosity fluids. This may explain why erosion ratios decrease as viscosity increases for each particle size.

Predicted particle speeds using two different meshes were analyzed and compared. It was found that grid sizes do not affect speeds for the meshes investigated.

CFD was utilized to predict erosion ratio for aluminum for particle sizes of 20, 150, and 300 µm in carrier fluids of 1, 10, 25 and 50 cP. The comparison of predicted and measured erosion ratios of aluminum 6061-T6 showed that CFD tends to significantly (by a factor of approximately 2 to 10) underpredict erosion ratio for 150 and 300 µm particles.

For 150 μm particles, the trend of predicted erosion ratio is comparable to that of the measured erosion ratio. For the 20 μm sand, the predicted erosion ratio decreases from 1 to 10 cP but increases from 10 to 50 cP which does not agree with the experimental data. It was also observed that erosion ratio is overpredicted for 20 μm particles.

The number of particles impacting the wall or target material was studied using CFD simulations. It was found that particles in higher viscosity fluids impact the wall more frequently than particles in lower viscosity fluids. It was also found that 20 micron particles tend to impinge the target over and over again resulting in large predicted erosion ratio while 150 and 300 micron particles only impact a few times and exit the region of interest near the wall. The erosion ratios of 20 micron particles were recalculated using information from only the first impact of each impacting particle. The predicted erosion ratio using only the first impact successfully agrees with the trend of the observed erosion ratio of the experimental data. This implies that the number of impacting particles is another important factor for erosion prediction.

Although CFD tends to underpredict the measurements for sand in viscous liquids, it is able to predict particle speed and erosion ratio which match the trend of measured speed and erosion ratio. Overall, CFD is capable of being used as a tool to predict erosion. It should be mentioned that the erosion equations used in this study were all generated from gas data for a range of speeds from 13 to 42 m/s. However, the magnitude of erosion did not match the data for sand in viscous liquids. Therefore, some modifications may be needed if there is a fundamental factor causing differences in erosion process in liquids and gases.

7. REFERENCES

[1] Finnie, I., McFadden, D., "On the speed dependence of the erosion of ductile metals by solid particles at low angles of incidence", Wear 48 (1978) 181–190.

[2] McLaury, B., “A Model to Predict Solid Particle Erosion in Oilfield Geometries”, Masters of Science Thesis, The University of Tulsa, 1993.

[3] Oka, Y.I., Okamura, K., Yoshida, T., “Practical Estimation of Erosion Damage caused by Solid Particle Impact, Part 1: Effects of Impact Parameters on a Predictive Equation”, Wear, 259, 2005.

[4] Oka, Y.I., Yoshida, T., “Practical Estimation of Erosion Damage caused by Solid Particle Impact, Part 2: Mechanical Properties of Materials directly associated with Erosion Damage", Wear, 259, 2005.

[5] Zhang, Y., "Application and Improvement of Computational Fluid Dynamics (CFD) in Solid Particle Erosion Modeling", Doctorate of Philosophy Dissertation, The University of Tulsa, 2006.

[6] Zhang, Y., Reuterfors, E.P., MClaury, B.S., Shirazi, S.A., Rybicki, E.F., "Comparison of Computed and Measured Particle Speeds and Erosion in Water and Air Flows", Wear, 263, 2007.

[7] Zhang, Y., Okita, R., Miska, S., McLaury, B.S., Shirazi, S.A., Rybicki, E.F., “CFD prediction and LDV validation of liquid and particle speeds in a submerged jet impinging a flat surface for different viscosities and particle sizes”, Proceedings of ASME 2009 Fluids Engineering Division, Vail, Colorado, August 2009.

[8] Miska, S., "Particle and Fluid Speed Measurements for Viscous Liquids in a Direct Impingement Flow Resulting in Material Erosion", Masters of Science Thesis, The University of Tulsa, 2008.

[9] Torabzadehkhorasani, S., "Erosion Experiments and Calculations in Gas and Liquid Impacts Varying Particle Size and Viscosity", Masters of Science Thesis, The University of Tulsa, 2009.

[10] Finnie, I., "Some observations on the erosion of ductile materials", Wear, 19, 1972.

[11] Meng, H.S., Ludema, K.C., “Wear models and predictive equations: their form and content”, Wear 181–183 (1995) 443–457.

[12] Lindsley, B.A., Marder, A.R., “The Effect of Speed on the Solid Particle Erosion Rate of Alloys”, Wear, 225-29, 1999.

[13] Oka, Y.I., Matsumura, M., Kawabata, T., “Relationship between Surface Hardness and Erosion Damage caused by Solid Particle Impact”, Wear, 162, 1993.

[14] Oka, Y.I., Ohnogi, H., Hosokawa, T., Matsumura, M., “The Impact Angle Dependence of Erosion Damage caused by Solid Particle Impact”, Wear, 203, 1997.